Causes of compositional diversity in a lobe of the Half Dome granodiorite, Tuolumne Batholith, Central Sierra Nevada, California

R. C. Economos[1], V. Memeti[1], S. R. Paterson[1], J. S. Miller[2], S. Erdmann[3] and J. Žák[4,5]

[1] University of Southern California, Department of Earth Sciences, 3651 Trousdale Parkway, Los Angeles, CA 90089–0740, USA
Email: economos@usc.edu

[2] Department of Geology, San José State University, San José, CA 95192–0102, USA

[3] Department of Earth Sciences, Dalhousie University, Halifax, Nova Scotia, B3H 4R2 Canada

[4] Institute of Geology and Paleontology, Charles University, Albertov 6, Prague, 12843, Czech Republic

[5] Czech Geological Survey, Klárov 3, Prague, 11821, Czech Republic

ABSTRACT: The causes of compositional diversity in the Tuolumne Batholith, whether source heterogeneity, magma mixing, or fractional crystallisation, is a matter of longstanding debate. This paper presents data from detailed mapping and a microstructural and major element, trace element and isotopic study of an elongate lobe of the Half Dome granodiorite that protrudes from the southern end of the batholith. The lobe is normally zoned from quartz diorite along the outer margin to high-silica leucogranite in the core. Contacts are steep and gradational, except for the central leucogranite contact, which is locally sharp: magmatic fabrics overprint contacts. A striking feature of the lobe is the 18 wt% SiO_2 range comparable to that observed for the entire Tuolumne Batholith. Feldspar-compatible elements (Sr and Ba) decrease towards the centre, while Rb increases. Light and middle REEs show a smooth decrease towards the centre of the lobe. Calculated initial isotopic ratios of $^{87}Sr/^{86}Sr_{(i)}$ and $\varepsilon Nd_{(t)}$ have identical values within error across the lobe, except in the central leucogranite, the most silica rich phase, which shows a slightly more crustal signature. Field, structural, geochemical and isotopic data suggest that fractionation was the dominant process causing compositional variation in this lobe. It is envisioned that this fractionation/crystal sorting occurred in a vertically flowing and evolving magma column with the present map pattern representing a cross-section of this column. Thus the areal extent of the lobe represents a minimum size of interconnected melt at the emplacement level of the Tuolumne Batholith and, given its marginal position, limited width and proximity to colder host rocks, implies that fractionation in larger chambers likely occurred in the main Tuolumne Batholith magma chamber(s).

KEY WORDS: fractional crystallisation, magmatic processes, plutons

The ~1100 km^2 Tuolumne Batholith in the central Sierra Nevada, California (Fig. 1), represents a spectacularly exposed, protracted record of plutonic assembly and internal differentiation in a large, open system continental arc magma chamber. Controversies over the assembly and internal differentiation processes in the Tuolumne Batholith persist, despite increasingly large geochronological and geochemical data sets collected from the batholith over the past 25 years. Central to this debate is the long-standing question of whether the compositional diversity preserved in the Tuolumne Batholith largely reflects source region heterogeneity, contamination, internal fractional crystallisation, or a combination of processes. Bateman & Chappell (1979) used geochemical data to argue that compositional diversity in the Tuolumne Batholith formed largely by *in situ* fractional crystallisation of a single, batholith-sized pulse. Kistler *et al.* (1986) used isotopic data to argue that much of the compositional diversity reflects mixing between two separate mantle and crustal derived melts. More recently, Coleman *et al.* (2004) and Glazner *et al.* (2004) argued that a 94–85 Ma intrusion interval requires growth of the Tuolumne Batholith by numerous small increments of magma, although the specific size and longevity of these increments remains contentious. In this model, compositional diversity and elemental variability in the batholith largely reflect variations in partial melt fraction and/or melt source heterogeneity. Based on field studies and published geochemistry, Paterson & Vernon (1995) Žák & Paterson (2006) and Memeti *et al.* (2007a) argued that the diversity was caused by the intrusion of large, nested diapirs derived from different source compositions and that fractional crystallisation occurred within these pulses, and mixing/mingling occurred along the margins between major pulses. The size and longevity of the pulses proposed by these authors was also not specified.

The above also highlights the issue of whether large magma chambers commonly exist in magmatic arcs and the size and number of pulses juxtaposed during batholith construction (Pitcher & Berger 1972; Hutton 1992; Lagarde *et al.* 1990;

 doi:10.1017/S1755691009016065

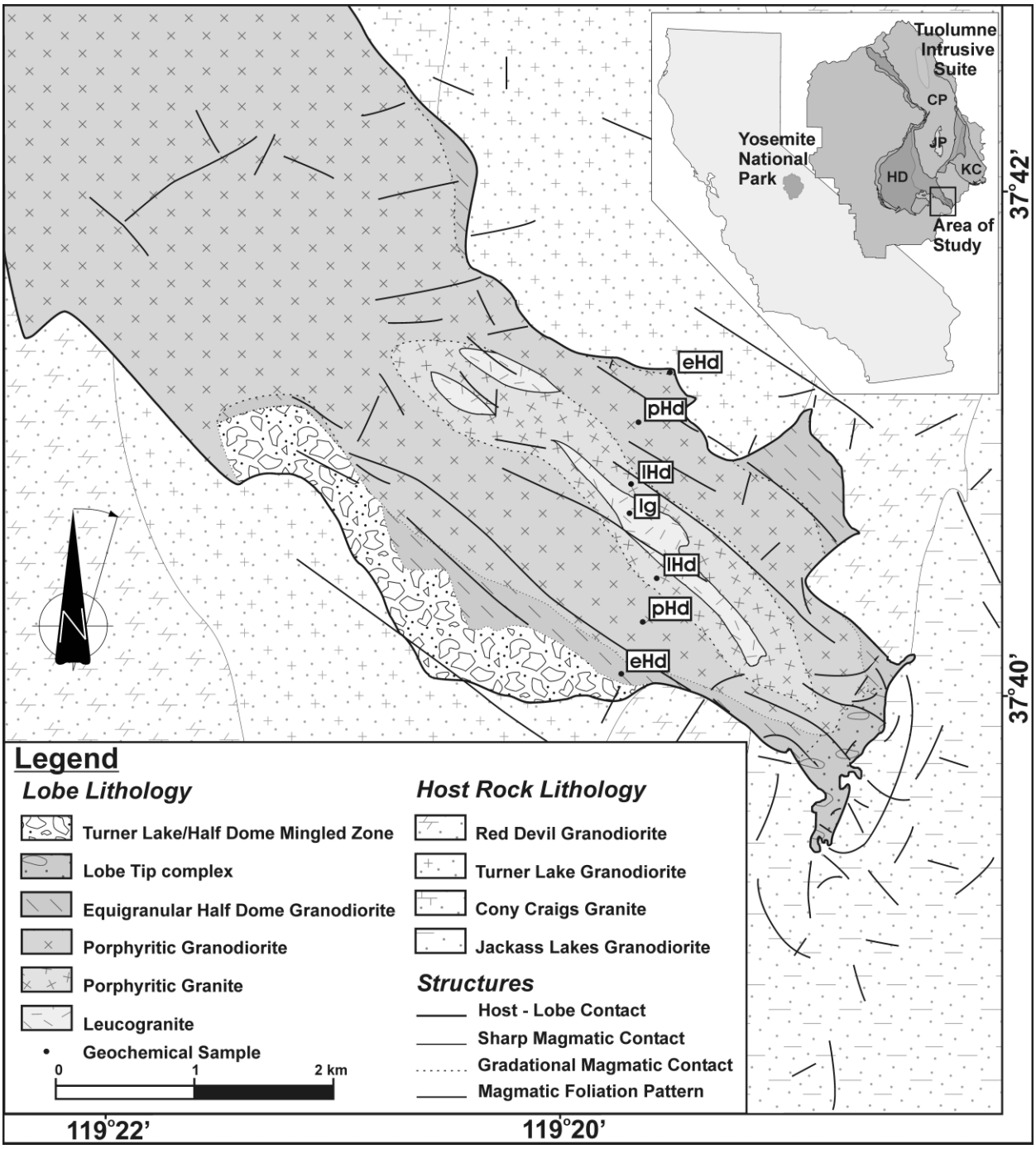

Figure 1 Map of the Half Dome granodiorite lobe and sample locations, with location maps of Yosemite National Park in CA and inset map of the Tuolumne Batholith. Main TIS units are labelled: Kuna Crest (KC); Half Dome (HD); Cathedral Peak (CP); Johnson Porphyry (JP). Lobe units are labelled: equigranular Half Dome granodiorite (eHd); porphyritic Half Dome granodiorite (pHd), leucocratic Half Dome granite to granodiorite (lHd); and leucogranite (lg).

Paterson & Miller 1998; Wiebe & Collins 1998; Johnson *et al.* 1999; Miller & Paterson 2001; Coleman *et al.* 2004; Matzel *et al.* 2005, 2007; Memeti *et al.* 2007b). It is suggested that a useful approach to address these issues is to examine magmatic lobes extending out from the main batholith (Memeti *et al.* 2005). Peripheral lobes in general may offer a relatively simple and short history, and may be more readily amenable to petrogenetic interpretation, in comparison to the larger domains that are complicated by reheating and juxtaposition of later pulses. (Memeti *et al.* 2005; Economos *et al.* 2005; Memeti *et al.* 2007a).

1. Geologic setting

The Tuolumne Batholith, emplaced at a depth of 6–10 km (Ague & Brimhall 1988; Webber *et al.* 2001; Gray 2003), is normally zoned from outer mafic units to inner, progressively more felsic units (Fig. 1) (Bateman 1992). The outer units include the 95–92 Ma Glen Aulin and Glacier Point tonalites and Kuna Crest granodiorite (Bateman 1992; Kistler & Fleck 1994; Coleman *et al.* 2004). Within these is the 91–88 Ma more siliceous Half Dome granodiorite which contains an outer equigranular unit and inner porphyritic unit with K-feldspar

https://doi.org/10.1017/S1755691009016065 Published online by Cambridge University Press

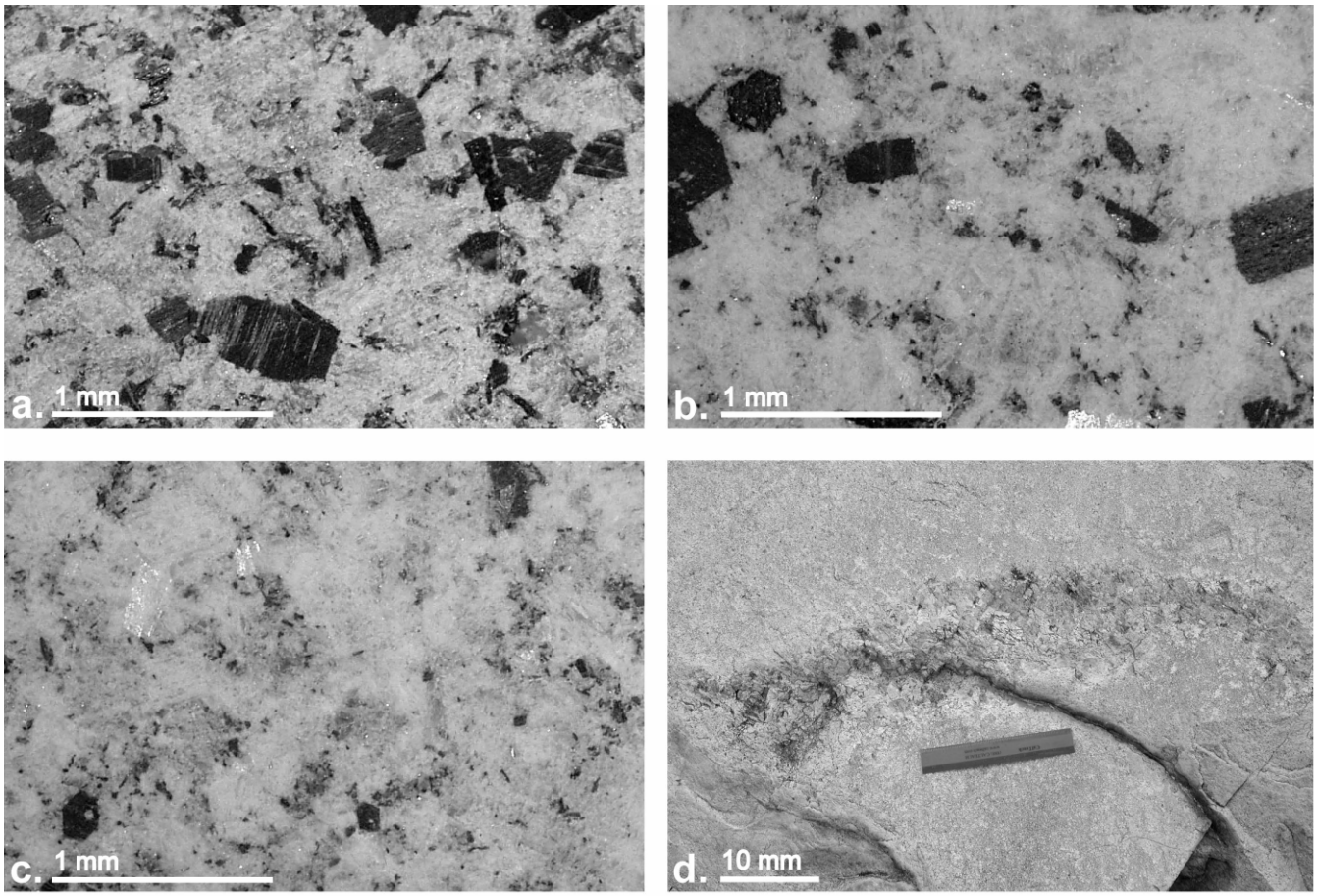

Figure 2 Photographs of Half Dome Lobe units: (a) Equigranular Half Dome granodiorite; (b) Porphyritic Half Dome granodiorite; (c) leucocratic porphyritic Half Dome granodiorite; (d) central leucogranite.

phenocrysts up to 3–4 cm in length (Bateman 1992; Kistler & Fleck 1994; Coleman *et al*. 2004). Further inward is the most aerially extensive unit in the batholith, the 88–85 Ma megacrystic Cathedral Peak granodiorite (Bateman 1992; Kistler and Fleck 1994; Coleman *et al*. 2004, Matzel *et al*. 2005). The small central phase is the ~87 Ma Johnson Granite Porphyry containing local Cathedral Peak inclusions and K-feldspar phenocrysts (Bateman 1992; Titus *et al*. 2005; Bracciali 2008).

This paper focuses on the Half Dome granodiorite. The most distinctive petrographic characteristics of this unit include approximately equal amounts of large (often >1 cm long) euhedral hornblendes and small subhedral biotites and prominent titanite crystals (Bateman 1992). The Half Dome unit dominates the southwestern portion of the main Tuolumne Batholith and has narrow northward and southward protruding lobes (Fig. 1 inset). The southern lobe was originally mapped as Half Dome granodiorite (Peck 1980; Huber *et al*. 1989), but was later assigned to the porphyritic Half Dome phase (Bateman 1992). The lobe intrudes the ~98 Ma Red Devil Lake granodiorite (Tobisch *et al*. 1995), the Turner Lake granite, and the Cony Craigs Porphyry (Bateman 1992). The southern tip of the lobe extends into the 97–98 Ma Jackass Lakes pluton (McNulty *et al*. 1996).

Thermal modelling and $^{40}Ar/^{39}Ar$ thermochronology indicate that the Half Dome lobe may have cooled in a few 10^5 years (Paterson *et al*. 2007), whether emplaced as a single or multiple pulses. An ongoing study of detailed U/Pb zircon geochronology in the lobe yields a 206 Pb/238 U ages of 90·12 ± 0·16 Ma (MSWD of 2·3) for the oldest phase (Fig. 1, 'pHd') and 89·68 ± 0·24 Ma for the youngest phase (Fig.1, 'lg') (Memeti *et al*. 2007c; Memeti *et al*. in press).

2. Results

2.1. Field relationships

The southern Half Dome lobe has been remapped at a 1:10 000 scale. The new mapping shows that the lobe can be divided into four compositionally and texturally distinct phases (Figs 1, 2). The outermost phase is a granodiorite to quartz monzodiorite that is generally equivalent to the equigranular variety of the Half Dome granodiorite in the main batholith (hereafter 'outer phase' [eHd]). It is medium-grained and contains up to 2 cm euhedral hornblende and up to 1 cm euhedral titanite (Figs 1, 2a). This phase grades inwards into a biotite-dominated, porphyritic granodiorite containing K-feldspar megacrysts up to 5 cm in length (hereafter, 'porphyritic phase' [pHd]) (Figs 1, 2b). This phase grades inwards to a more leucocratic, medium-grained biotite granodiorite to monzogranite with 0–2% modal hornblende, 3–5% modal biotite, and sparse, 1–3 cm K-feldspar megacrysts (hereafter, central phase [lHd]) (Figs 1, 2c). The innermost central phase is a fine-grained monzogranite dominated by quartz and K-feldspar with less than 1% modal biotite (hereafter, 'leucogranite' [lg]) (Figs 1, 2d). These units are organised in a symmetrical map pattern with NW-striking contacts aligned parallel to the margins of the lobe (Fig. 1); textural and compositional characteristics of units on the east and west sides of the lobe are identical.

Whilst the compositions within each phase are relatively homogeneous, contacts between the outer, porphyritic, and central phases are gradational over zones 50–60 m wide. As such, contact zones were characterised by gradual changes in

https://doi.org/10.1017/S1755691009016065 Published online by Cambridge University Press

modal mineralogy, microstructure and colour index, and defined in the field as the regions of largest gradients of the above. These gradational contacts remain subvertical across fairly significant changes in topography, and are thus interpreted to be steeply dipping everywhere within the lobe. Cross-cutting dikes from different phases reveal that the outer phase is the oldest, and that phases young towards the centre of the lobe. The contact between the leucogranite and its surrounding central phase is unusual in the lobe in that it is sharp in most localities and has both shallow and steep dips.

The contact between the lobe and its older plutonic host rocks varies dramatically in structure and composition along strike. The tip of the lobe exhibits a highly irregular pattern and is also structurally complex. Compositions range from granite to monzodiorite, with predominantly granodiorite compositions. This tip area contains many randomly oriented blocks of host rock granitic units and rhyolitic to dacitic metatuffs (observed only as blocks) ranging from centimetre- to tens of metres-scales. Enclave swarms tens of metres in diameter that contain hundreds of mafic enclaves are common. Dikes that cross cut host rocks extrude southward away from the very southern tip of the lobe. The southern lobe contact north of the tip is characterised by a 100–200 m-wide structurally complex zone between the equigranular Half Dome granodiorite and the Turner Lake granite (Fig. 1, 'Turner Lake/Half Dome mingled zone'). Common complexities along this contact include mingling between distinctive hornblende-free Turner Lake granite and Half Dome lobe granodiorite, blocks of Turner Lake granite surrounded by Half Dome granodiorite, and abundant schlieren. The northern lobe–host rock contact is generally sharp. Magmatic fabrics in the lobe include a ~NNW–SSE foliation and an ~E–W foliation that overprints all gradational internal contacts in the lobe (Fig. 1).

2.2. Petrography

The outer phase of the Half Dome lobe consists of 53–61% plagioclase, 12–22% quartz, 6% K-feldspar, 10% biotite and 7% hornblende. Accessory minerals include abundant 1·5–3 mm euhedral titanite, apatite, magnetite and zircon. Plagioclase, hornblende and biotite are sub- to euhedral. K-feldspars are large and anhedral, commonly showing perthite exsolution and appear to occupy interstices between more euhedral phases. Plagioclase and hornblende inclusions also commonly occur in K-feldspars. Myrmekite occurs in this phase, and chloritisation of biotites, undulose extinction in quartz and mild deformation of plagioclase twins are also observed.

The porphyritic phase contains 43–54% plagioclase, 20–28% quartz, 14% K-feldspar, 8% biotite and 3% hornblende. Accessory minerals include titanite, apatite, magnetite, zircon and allanite. Titanite is less abundant, but still large and euhedral. K-feldspars have a similar morphology to the outer phase and also show perthite texture, but are occasionally much larger, up to 1·5 cm in length.

The central phase contains 38% plagioclase, 28–32% quartz, 25–29% K-feldspar, 2–5% biotite, and 0–2% hornblende. Titanite and magnetite are present, but less abundant in this phase. K-feldspars are subhedral and perthitic. Whilst K-feldspars are still poikiolitic, they no longer display the interstitial texture from outer phases. Zircon and apatite are also common accessory phases.

The leucogranite phase contains 35% plagioclase, 48% quartz, 16% K-feldspar, and 1% biotite. Titanite is far less abundant than in other phases and is subhedral. Grain sizes in the leucogranite phase are equigranular and markedly smaller than in other phases. Alteration is much more prevalent in this phase, including complete chloritisation of biotite and strong sericitisation of plagioclase crystals. Minor sulfides also occur in this unit.

In summary, modal mineralogy in the lobe shows a clear increase in quartz content and a decrease in plagioclase, hornblende, biotite and titanite toward the centre of the lobe. Total K-feldspar content increases inward and peaks in the megacryst bearing phase.

2.3. Geochemistry

Seven samples for geochemical analyses were collected along a N–S transect across the dominantly NE–SW zoning in the lobe (Fig. 1, Table 1). Samples representative of the main units were selected for analyses.

Whole rock major and trace element data were collected by X-ray flourescence (XRF) and inductively coupled plasma mass spectrometer (ICP-MS) at the Geoanalytical laboratory at Washington State University. Sample chips were selected and ground in a tungsten carbide mill, mixed with dilithium tetraborate, and fused in graphite crucibles for major element analysis and some minor elements. REE analyses of low abundance trace elements were analysed on a quadrupole mass spectrometer with an inductively coupled argon plasma source. Detection limits were at or below chondrite levels. Samples for ICP-MS analysis were ground in an iron bowl in a shatterbox swing mill. Two grams of rock powder were mixed with an equal amount of lithium tetraborate flux, placed into a carbon crucible and fused. The resulting fused bead was re-ground and dissolved in a mixture of HF, HNO_3, and $HCLO_4$. The samples were then dried and re-dissolved and mixed with a standard of In, Re and Ru, used to correct for instrument drift. Measurements were conducted on a Sciex Elan model 250 ICP-MS. Calibration curves were constructed from common silicate rock standards run with the samples for each element and unknown concentrations were computed from these curves.

Whole-rock Nd and Sr isotopic data were also collected for each phase of the lobe (Fig. 3e, f, Table 2). Two hundred mg of rock powder for each sample was dissolved in a mixture of HF and HNO_3 and spiked with mixed ^{150}Nd-^{147}Sm spike in a sealed Teflon bomb at 180°C for 5–7 days. Separation of Rb, Sr and the REE group followed standard cation-exchange procedures. Separation of Sm and Nd used alpha-HIBA on cation exchange resin. Strontium was separated using Sr-spec column chemistry and HNO_3. Neodymium was loaded on single Re filaments with dilute HCl, and Sm were loaded on single-Ta filaments with H_3PO_4. Strontium was loaded with H_3PO_4 and $TaCl_5$ emitter on a single Re filament. All analyses were performed on the Micromass Sector-54 mass spectrometer at the University of North Carolina. Neodymium was analysed in dynamic multicollector mode as NdO using an oxygen bleed valve at 1V, and Sm was analysed in static multicollector mode with $^{147}Sm = 200$ mV. Strontium was analysed in dynamic multicollector mode with $^{88}Sr = 3V$. Neodymium data are normalised to $^{146}Nd/^{144}Nd = 0{\cdot}7219$. Strontium data are normalised to $^{86}Sr/^{88}Sr = 0{\cdot}1194$. During the period of analysis, replication of SRM-987 yielded $^{87}Sr/^{86}Sr = 0{\cdot}710246 \pm 0{\cdot}000010$. Nd data are referenced to La Jolla Nd ($^{143}Nd/^{144}Nd = 0{\cdot}511853$). Replicate analysis of the UNC J-Nd standard during the period of analysis gave $^{143}Nd/^{144}Nd = 0{\cdot}512099 \pm 0{\cdot}000005$. This internal standard is also referenced to LaJolla Nd but is run more frequently. No bias correction has been applied based on repeated measurements of both standards. Initial Sr ratios were calculated using $\lambda^{87}Rb = 1{\cdot}42 \times 10^{-11}$ yr, and using Rb and Sr concentrations measured by ICP-MS. Initial ratios are calculated using a nominal age of 92 Ma for the Half Dome granodiorite (e.g. Coleman *et al.* 2004).

https://doi.org/10.1017/S1755691009016065 Published online by Cambridge University Press

Table 1 Major oxide and trace element data collected at the Geoanalytic Laboratory at Washington State University. Major oxides were measured by XRF and trace elements were measured by ICP-MS.

XRF measurements in wt%:

Sample	SiO_2	AI_2O_3	CaO	MgO	Na_2O	K_2O	Fe_2O_3	MnO	TiO_2	P_2O_5	Cr_2O_3	LOI	Sum
1	58·22	17·97	5·78	2·4	4·17	2·46	6·26	0·11	0·87	0·29	0·02	0·45	98·99
2	67·2	15·88	3·37	0·99	4·17	3·36	3·37	0·07	0·48	0·18	0·02	0·25	99·32
3	74·9	12·9	1·19	0·25	3·28	4·57	1·35	0·02	0·14	0·04	0·03	0·3	98·97
4	76·17	12·86	0·88	0·11	3·57	4·49	1·14	0·02	0·09	0·01	0·03	0·1	99·47
5	68·74	15·44	2·99	0·78	3·97	3·53	2·87	0·06	0·43	0·15	0·02	0·4	99·38
6	66·68	15·9	3·37	1·02	4·04	3·15	3·51	0·07	0·49	0·17	0·02	0·45	98·86
7	61·7	16·17	4·93	1·98	3·73	2·81	5·57	0·09	0·75	0·27	0·02	0·4	98·42

ICP-MS measurements:

Sample	Li (ppm)	Mg (%)	P (%)	Cr (ppm)	Fe (%)	Ni (ppm)	Rb (ppm)	Sr (ppm)	Y (ppm)	Zr (ppm)	Nb (ppm)	Cs (ppm)	Ba (ppm)
1	26	1·52	0·14	114	4·16	10	93·9	872·4	12·6	77·5	9	3·3	889·6
2	26	0·62	0·09	137	2·28	9	130·5	697·2	7·2	124·8	7	5·7	1119·6
3	16	0·14	0·02	182	0·92	8	192·9	151·4	2·4	60·5	5	6·4	194
4	<10	0·06	<0·01	181	0·78	<5	205·4	72·6	2·2	56·8	7	3·9	45·5
5	23	0·48	0·07	127	1·9	7	139·8	624·6	6·2	73·2	7	6·7	825·4
6	26	0·66	0·08	150	2·42	9	118·1	679·1	7·9	138·9	7	4·7	926·5
7	19	1·28	0·12	134	3·84	13	86·2	797·2	11·3	115·1	9	3·8	1107·3

Sample	La (ppm)	Ce (ppm)	Pr (ppm)	Nd (ppm)	Sm (ppm)	Eu (ppm)	Gd (ppm)	Tb (ppm)	Dy (ppm)	Ho (ppm)	Er (ppm)	Tm (ppm)	Lu (ppm)
1	32	63·5	7·36	27·5	4·8	1·24	4·28	0·58	2·4	0·47	1·21	0·17	0·22
2	25·1	46·1	5·29	19·6	3	0·86	2·68	0·37	1·5	0·27	0·78	0·1	0·13
3	15·7	18·9	1·55	4·7	0·7	0·18	0·58	0·08	0·35	0·08	0·2	<0·05	0·08
4	17·1	17·1	1·24	3·4	0·5	0·08	0·47	0·06	0·31	0·07	0·25	<0·05	0·06
5	22·5	40·5	4·92	17·5	2·7	0·77	2·26	0·29	1·16	0·21	0·59	0·08	0·12
6	26·4	48	5·59	20·6	3·4	0·85	2·74	0·36	1·47	0·28	0·79	0·12	0·13
7	29·3	59·2	7·25	27·2	4·5	1·11	3·83	0·49	2·1	0·39	1·23	0·16	0·17

Sample	Yb (ppm)	Hf (ppm)	Pb (ppm)	Th (ppm)	U (ppm)
1	1·1	3	13	11·3	7·92
2	0·7	4	52	11·8	3·84
3	0·3	3	24	19·4	6·12
4	0·3	3	67	21	6·52
5	0·5	2	17	17·1	4·02
6	0·7	4	15	13·3	3·68
7	1	3	13	11·8	4·66

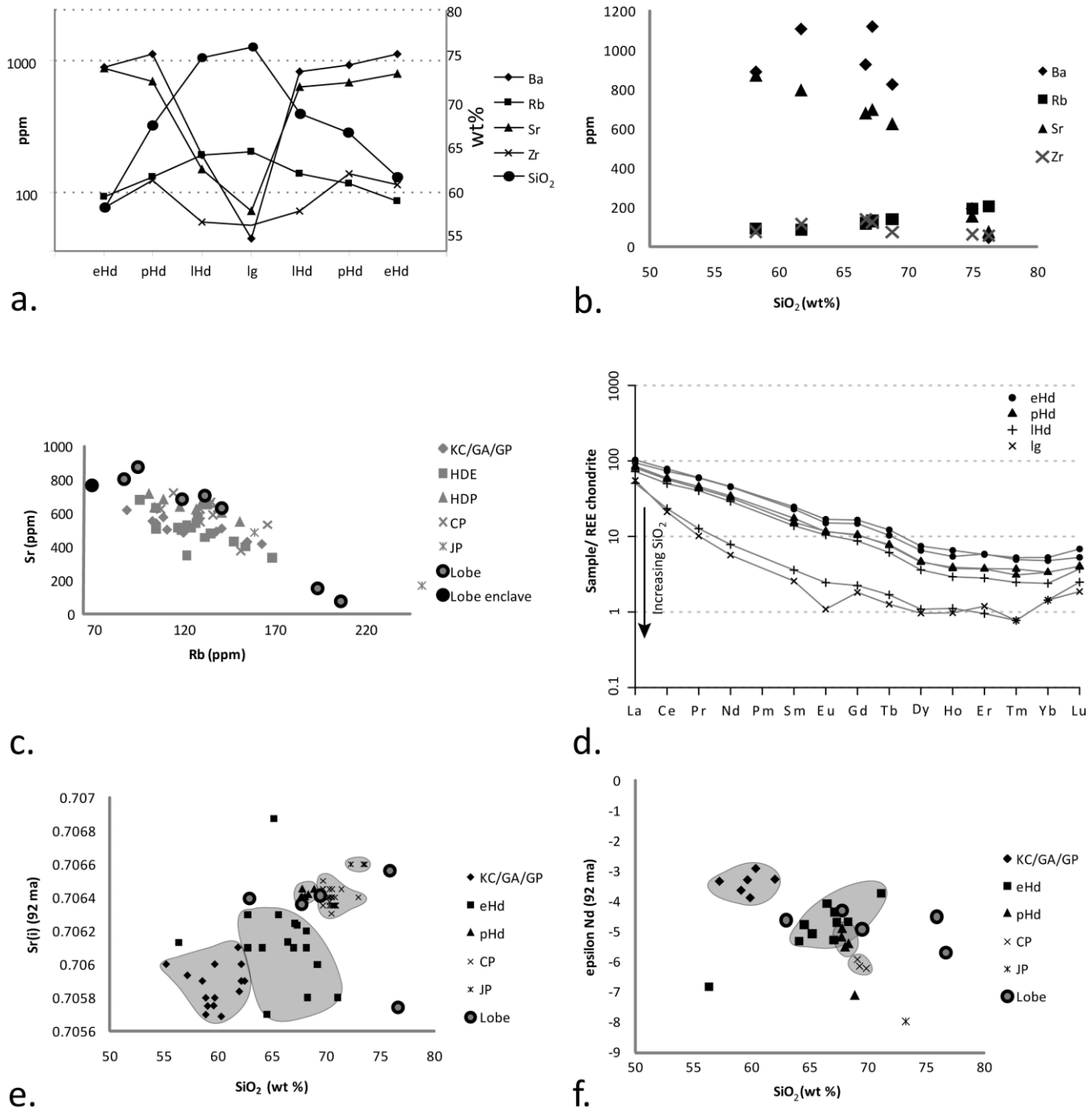

Figure 3 (a) Trace elements Ba, Sr, Rb, Zr and SiO_2 plotted across the lobe to demonstrate symmetrical pattern; (b) The same trace elements plotted against SiO_2; (c) Sr vs. Rb for the Half Dome lobe and the entire Tuolumne Batholith (Bateman & Chappell 1979; Bateman 1992; Gray 2003); (d) Rare Earth Elements normalised to chondrite (Boynton 1984); (e) (f) Sr(i) and εNd vs. SiO_2 for the Tuolumne Batholith (Gray 2003; Kistler *et al.* 1986) and the Half Dome lobe.

The compositional and textural symmetry of the lobe is strongly reflected in geochemical trends. SiO_2 content across the lobe displays a symmetrical inward increase from ~60 wt% SiO_2 in the outer phase to 76 wt% SiO_2 in the leucogranite phase (Fig. 3a). This SiO_2 range is impressive, since it is as large as that of all four mapped units of the main batholith combined (Bateman & Chappell 1979). All major oxide trends in both the lobe and the main batholith show fairly linear relationships with SiO_2 with very little scatter (Bateman & Chappell 1979). CIPW norm calculations (including hornblende) confirm the mineralogical trends identified through point counting, including an increase in K-feldspar in the porphyritic phase of the lobe.

Trace element analyses reveal a symmetrical increase in Rb content towards the centre of the lobe, whereas Ba and Sr decrease toward the centre of the lobe with a major drop off in the leucogranite phase (Fig. 3a). When plotted against SiO_2, Rb and Sr show curvilinear trends, while Ba is more scattered (Fig. 3b). These trace element variations are unlike trends in the main batholith, which tend to show weak or no correlations with SiO_2 (Kistler *et al.* 1986; Fig. 2). Zr displays a more complex trend, increasing from the outer phase to the porphyritic phase and then dropping steeply across the gradational contact between the porphyritic phase and the central phase (Figs 3a, 4a, b). All REE concentrations decrease, with increasing SiO_2 toward the centre of the lobe. Light REEs are more

https://doi.org/10.1017/S1755691009016065 Published online by Cambridge University Press

Table 2 $^{87}Sr/^{86}Sr$ and $^{143}Nd/^{144}Nd$ are measured ratios with 2-sigma analytical errors in parentheses. Initial Sr and Nd ratios are calculated using an age of 92 Ma. Epsilon Nd values at the crystallisation age are calculated using $^{143}Nd/^{144}Nd_{(CHUR,\ 0\ Ma)}=0{\cdot}512638$ and $^{147}Sm/^{144}Nd_{(CHUR,\ 0\ Ma)}=0{\cdot}1967$. Rb and Sr concentration data determined by ICP-MS and Sm and Nd concentration data determined by isotope dilution. Errors in Rb and Sr are within 1% and 0·1% respectively of the amount present. Errors for Sm and Nd are within 2% of the amount present and epsilon values calculated using Sm/Nd from ICP data are within 5% of those calculated by ID-TIMS. Based on these considerations and replication of standards and rocks (e.g. BCR-1; see Miller *et al*. 2000), conservative errors of ± 0·00005 are assigned to initial $^{87}Sr/^{86}Sr$ and ± 0·5 epsilon units to initial εNd values.

Sample	Rb ppm	Sr ppm	$^{87}Sr/^{86}Sr$	$^{87}Sr/^{86}Sr$ (92)	Sm ppm	Nd ppm	$^{147}Sm/^{144}Nd$	$^{143}Nd/^{144}Nd$	εNd (92)	T_{DM} (Ma)
3	193	151	0·711382 (16)	0·706556	0·841	5·642	0·0901	0·512342 (65)	− 4·53	871
4	205	73	0·716378 (14)	0·705776	0·427	2·975	0·0867	0·512280 (09)	− 5·70	921
5	138	623	0·707197 (16)	0·706361	3·35	20·62	0·0981	0·512326 (09)	− 4·93	950
6	118	679	0·707068 (16)	0·706412	3·21	22·89	0·0848	0·512349 (08)	− 4·33	823
7	86	797	0·706802 (16)	0·706395	5·27	30·86	0·1032	0·512344 (12)	− 4·63	970

enriched than heavy REEs in all samples, and light REE enrichment relative to heavy REEs becomes more pronounced in the central phases (Fig. 3d). Middle REEs show a decrease, particularly in the core aplite, and have a 'scooped' shape that is characteristic of other titanite-bearing Sierran aplites (Glazner *et al*. 2008).

Initial Sr and Nd isotopic compositions (and $\varepsilon Nd_{(t)}$) are invariant within error for the outer, porphyritic and central phases (spanning 15 wt% silica) with $^{87}Sr/^{86}Sr_{(i)}=0{\cdot}7064$ and $\varepsilon Nd_{(t)}=-4{\cdot}6$ (Fig. 3e, f). The leucogranite unit has $^{87}Sr/^{86}Sr_{(i)}=0{\cdot}7058$ and $\varepsilon Nd_{(t)}=-5{\cdot}8$, and is therefore isotopically distinct from the other units.

3. Discussion

A robust petrogenetic model for the southern Half Dome lobe must address: (1) normal zoning from mafic/intermediate to felsic that is symmetrical from margin to centre; (2) gradational, steeply dipping magmatic contacts between all units and sharp and variably dipping contacts with the leucogranite; (3) hornblende-rich 'cumulate-like' zones and local layering and associated mafic enclave swarms at the margin of the lobe; (4) smooth decreases in plagioclase and mafic mineral content and appearance of K-feldspar phenocrysts across a narrow gradational zone; (5) smooth and linear major element variation (excluding Na_2O) with SiO_2; (6) regular trace element variation with SiO_2 and distance for many trace elements (Fig. 3a, b); and (7) invariant Nd and Sr isotopic composition across a wide range of SiO_2 and with distance from the lobe margins with a minor variation in the core leucogranite (Fig. 3e, f).

The symmetric zoning pattern is one of the key compositional aspects of the Half Dome lobe that distinguishes it from the Half Dome elsewhere in the Tuolumne. For example, the much larger mass of the Half Dome granodiorite that comprises most of the southwestern exposure of the Tuolumne (see Fig. 1 inset) is quite homogeneous in mineralogy and major element composition (Gray 2003). In addition, the contacts in the Half Dome lobe are everywhere gradational and are thus markedly simpler than those between the major mapped units in the main batholith, which may change from gradational to sharp along strike (e.g. Bateman 1992).

Compositional zoning of plutons has been attributed to a wide variety of processes including: crystal-liquid fractionation, mixing of compositionally different melts, restite unmixing, and emplacement of compositionally distinct pulses at a more or less constant locus of intrusion (cf. Ragland & Butler 1972; Bateman & Nokelberg 1978; Bateman & Chappell 1979; Halliday *et al*. 1980; Reid *et al*. 1983; Scambos *et al*. 1986; Hill *et al*. 1988; Sawka *et al*. 1990; Walawender *et al*. 1990; Barbey *et al*. 2001; Wyborn *et al*. 2001).

Given the field and petrologic data presented above it is considered unlikely that the lobe was emplaced with abundant restite and/or that restite unmixing was important (e.g., Miller *et al*. 2007). Magma mixing can occur between basaltic melts and felsic melts derived by remelting of mafic underplated materials (e.g. Coleman *et al*. 1992; 1995; Ratajeski *et al*. 2001), and so it cannot be unequivocally ruled out by isotopic data alone. The strikingly linear major element covariation and strong linear correlations with bulk composition are what might be expected for magma mixing, but they could also result from bulk unmixing in the lobe. Magma mixing between the enclave-forming mafic magma with any of the more felsic magmas is precluded by trace element trends (e.g. Rb vs. Sr, Fig. 3c), which clearly show that the enclave has too low Sr to serve as an appropriate mafic end member. Several trace elements display non-linear or curvilinear co-variations (Fig. 4c, d) that preclude a simple two component mixing model. Another first order constraint comes from the whole rock isotopic data, which, for all phases but the central aplite, excludes mixing of melts from two isotopically different sources. This suggests a relatively 'closed-system' process.

Along the margins of the lobe, evidence for the operation of crystal–liquid fractionation processes is indicated by the hornblende and biotite dominated zones and development of schlieren troughs and tubes (e.g. Weinberg *et al*. 2001; Žák & Paterson 2005). Away from the margins of the lobe, where transitions between phases are gradational, outcrop-scale evidence for these processes are also observed in the form of crystal accumulations and crystal-poor leucocratic veins (Paterson *et al*. 2005). These rocks have not been analysed, but within the Half Dome lobe they are the ones most obviously affected by accumulation and/or melt segregation. Their relatively minor volumetric proportion suggests that they are unlikely to form a primary cumulate assemblage for the lobe, and such rocks elsewhere in the Tuolumne Batholith cannot be easily related to the main geochemical trends (Reid *et al*. 1983; Paterson *et al*. 2008). They nevertheless provide evidence for redistribution of crystals and melt, and they are thus regarded as evidence for the operation of at least local crystal-melt movements in a magma chamber at the site of emplacement of the lobe.

All petrographic evidence is also permissive of fractional crystallisation, including increasing quartz and K-feldspar content towards the centre of the lobe and decreasing total plagioclase content. Overgrowth relationships show transitions from clinopyroxene to hornblende to biotite. The leucogranite phase represents a highly evolved melt. A simple least-squares mixing analysis of major element compositions revealed that approximately equal proportions of a residual outer phase and a leucocratic central phase would be produced by fractionating

https://doi.org/10.1017/S1755691009016065 Published online by Cambridge University Press

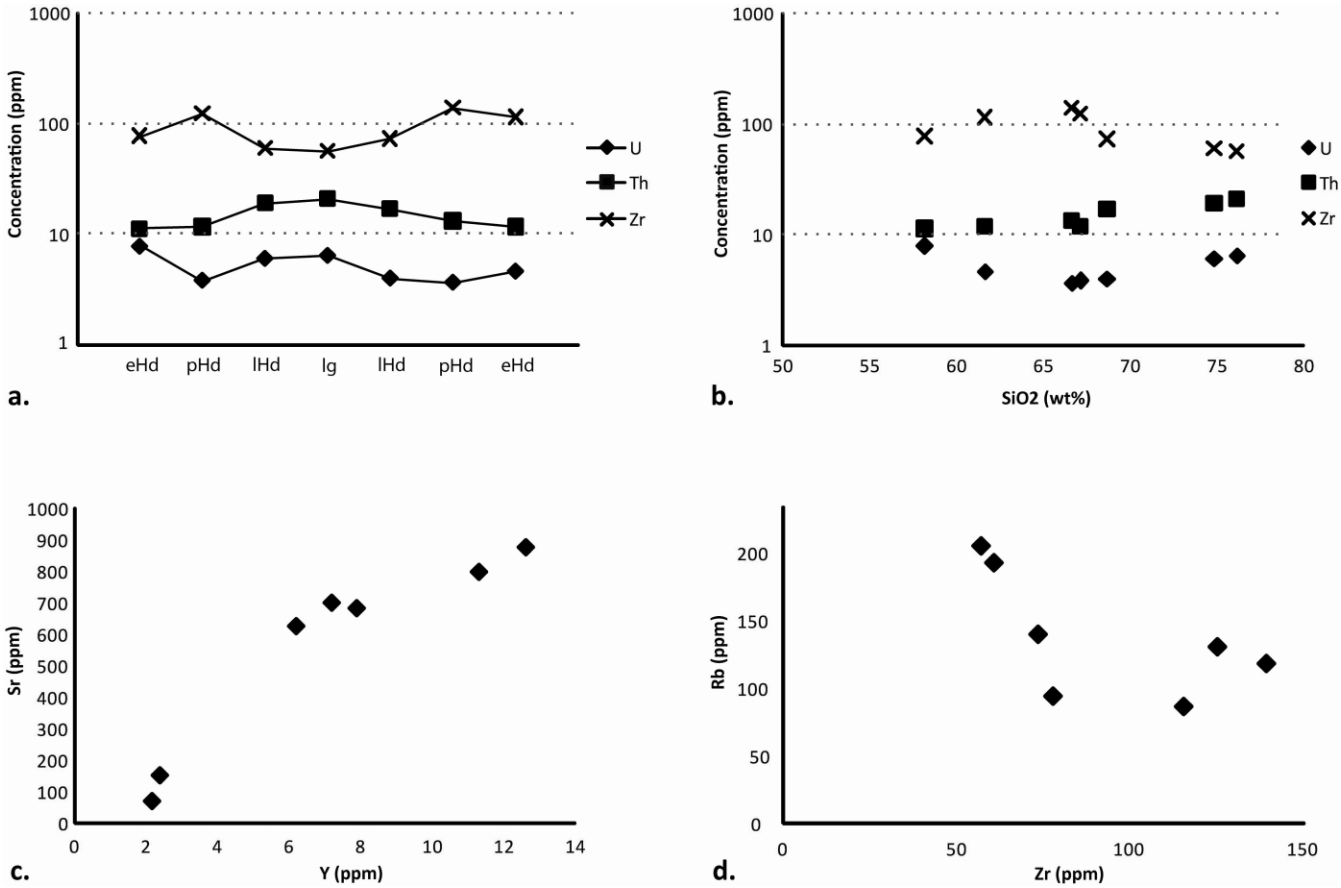

Figure 4 (a) Zircon related elements, U, Th, and Zr, plotted across the lobe showing an inflection point in the porphyritic unit; (b) the same elements plotted vs. SiO_2. (c) (d) Two examples of non-linear trace element trends in the Half Dome lobe: Y vs. Sr and Zr vs. Rb.

the porphyritic phase. However, not enough of the outer phase is present at the level of exposure to account for the fractionation of both the central and leucocratic phase. This is one of several observations that lead the present authors to propose a vertically evolving fractionation system in which some residue resides below the present level of exposure.

Trace element variations are also consistent with fractional crystallisation. Incompatible elements like Rb show an increase with SiO_2 and distance from the host rock contacts, whilst more compatible elements like Sr show a decrease (Fig. 3a), attributed to fractional crystallisation of the major minerals, such as hornblende and plagioclase. These minerals are found in higher abundances in the more marginal phases of the lobe. The pronounced drops in Sr and Ba observed in the leucogranite phase are controlled by feldspar fractional crystallisation, especially K-feldspar, again confirmed by changes in modal mineralogy (Figs 2, 3).

A modest increase in the Ce/Yb ratio is probably indicative of hornblende control until higher SiO_2 values are reached in the interior phases, whereupon Ce/Yb drops markedly. This likely reflects saturation and removal of phase(s) that strongly concentrate the light to middle rare earth elements, and extraction of melt that has been depleted in these elements. The removal of middle REEs that produces the distinctive 'scoop' shape of the rare earth element trend in the leucocratic phases of the lobe is likely attributable to accessory mineral fractional crystallisation, especially titanite (e.g. Glazner *et al.* 2008).

Finally, it is re-emphasised that the isotopic data are a strong indication for dominantly closed-system fractional crystallisation occurring in the Half Dome lobe. Both $^{87}Sr/^{86}Sr_{(i)}$ and $\varepsilon Nd_{(t)}$ values are equal to each other within error over an impressively large variation in SiO_2 content (Fig. 3e, f). This isotopic dataset bears striking similarity to field data, particularly contact relationships. Units that share gradational contacts have identical isotopic values, whilst the single unit with a sharp contact shows a slight isotopic shift.

Geochemical modelling to test the above hypotheses is underway. However, such modelling remains fairly non unique without detailed mineral geochemistry, full consideration of both major, trace, REE, and isotopic data and the roles/volumes of both major and accessory minerals and models designed to test all likely scenarios, and thus is beyond the scope of this paper. Another challenge for geochemical modelling, including modelling of the Tuolumne Batholith, is the increased evidence of recycling and mixing of crystal populations such as now documented for the zircon populations (Matzel *et al.* 2005; Miller *et al.* 2007) and established even at the mesoscale (Paterson *et al.* 2008).

Until these modelling studies are complete, the preferred interpretation is that the lobe represents a frozen cross-section of a vertically evolving and fractionating magma system (Fig. 5). This would allow the possibility that not all of the present exposure in the lobe was laterally connected melt at one time; but if not laterally, it was so vertically. Whilst the percentage of crystallisation beyond the formation of a crystal network is difficult to ascertain, modelling by Bachmann & Bergantz (2004) indicates that relatively crystal-poor magmas can be removed from a mush of 40% to >50% crystals.

The present authors envision a smaller scale version of the upper portions of models presented by Sisson (2005) and Ratajeski *et al.* (2005), in which crystal mush zones along conduit walls grade into a more upwardly mobile crystal mush centre. The chemical gradients, implying chemical communication between magma, cumulates at the host rock contact,

https://doi.org/10.1017/S1755691009016065 Published online by Cambridge University Press

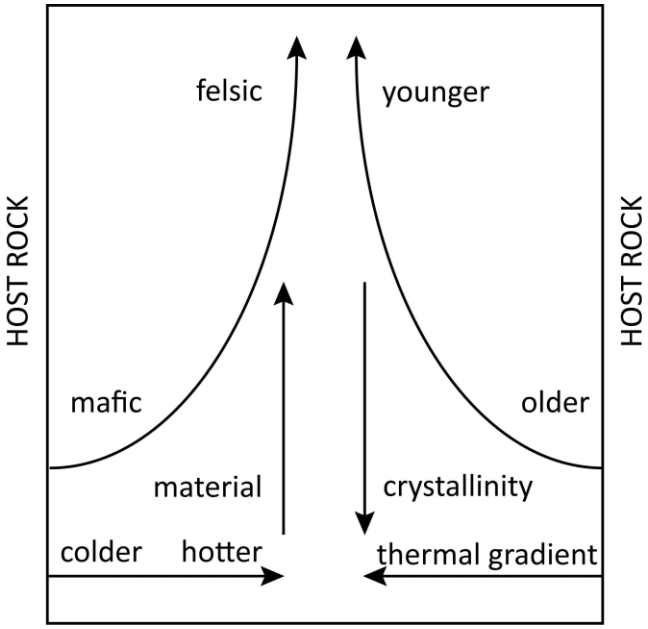

Figure 5 Schematic depicting the major boundary conditions envisioned for a vertically evolving column of fractionating material.

and overprinting magmatic fabrics in this lobe are all time-transgressive (both laterally and vertically); features consistent with this model. Thus, the compositional diversity in the lobe is generated by processes occurring both at and below the level of emplacement, but these processes are linked to each other by interconnected melt in an evolving system. If a similar system operated in the main batholith, in which pulses were disrupted by later intrusions, this nicely explains the difference in isotopic systematics between the Half Dome lobe and the entire Half Dome unit, with the former being isotopically homogeneous while the latter shows a much more complex history (Kistler *et al*. 1986; Kistler & Fleck 1994, Memeti *et al*. 2007b; Matzel *et al*. 2007).

Such a vertically evolving, fractionating system would predict the same or more likely even greater vertical extent than the cross-sectional area of the lobe. If such a volume of interconnected melt is achieved in the thermally less favourable environment of the lobe, larger bodies of interconnected melt should be expected within the main body of the Tuolumne Batholith. This conclusion is supported in the main batholith by magmatic fabrics that overprint all internal contacts (Žák *et al*. 2007), broad zones of mixing/mingling along these contacts and gradations between them (Bateman 1992; Žák & Paterson 2006; Paterson *et al*. 2008), and broad zones of nearly identical U/Pb zircon ages and related geochemistry in the large central Cathedral Peak unit (Burgess & Miller 2008).

One interesting question is why the major oxide diversity in the lobe is greater than that preserved in any unit in the main batholith. Was this signal somehow removed in the main batholith? Or if never achieved by an individual unit in the main batholith, does it imply that the elevated geothermal gradient and rapid crystallisation predicted in the lobes may produce more rather than less fractional crystallisation in natural systems? The most critical differences in boundary conditions between the lobe and the main batholith are thermal gradient during crystallisation (Spera & Bohrson 2001; Paterson *et al*. 2003; Memeti *et al*. 2007a) and presence of additional distinct magma pulses in the main batholith (Spera & Bohrson 2001). The effects of these boundary condition differences on the mechanical separation of crystals and liquid warrants additional discussion.

4. Conclusions

The mapping, structural, chemical and isotopic evidence suggests that a vertically flowing and fractionating column of magma, derived from a largely isotopically homogeneous source, played the dominant role in the formation of compositional diversity in the southern Half Dome granodiorite lobe of the Tuolumne Batholith. This keeps open the possibility that fractional crystallisation may have occurred in the main chamber over length and volume scales significantly larger than that of the lobe, requiring bodies of interconnected melt at least as large as the lobe at the time of emplacement of units in the main batholith.

These results suggest that fractional crystallisation at or near the level of emplacement of the Tuolumne Batholith is capable of producing major oxide heterogeneity of the magnitude seen in the entire batholith. Why this level of fractional crystallisation is not preserved in the main batholith may be that it is masked by subsequent processes (Memeti *et al*. 2007b), or that an elevated thermal gradient in the lobe was a driving factor for the degree of fractional crystallisation. A lower thermal gradient and juxtaposition of different batches in the main batholith may have allowed mixing to play a more significant role.

5. Acknowledgements

This work was supported by funds from the University of Southern California Department of Earth Sciences, by NSF grant EAR-0073943 (to Paterson), NSF EAR-0074099 (to Miller) and by Czech Academy of Sciences Grant No. KJB 3111403 (to Žák). Special thanks to J. Lawford Anderson for his intellectual contribution, and to Claire Wilke and Gayle Hough for their assistance in the field. Thanks to Dr Calvin Miller and Dr Allen Glazner for their constructive, helpful reviews.

6. References

Ague, J. J. & Brimhall, G. H. 1988. Magmatic arc asymmetry and distribution of anomalous plutonic belts in the batholiths of California; effects of assimilation, crustal thickness, and depth of crystallization. *Geological Society of America Bulletin* **100**, 912–27.

Bachmann, O. & Bergantz, G. W. 2004. On the origin of crystal-poor rhyolites extracted from batholithic crystal mushes. *Journal of Petrology* **45** (8), 1565–82.

Barbey, P., Nachit, H. & Pons, J. 2001. Magma–host interactions during differentiation and emplacement of a shallow-level, zoned granitic pluton Tarçouate pluton, Morocco: implications for magma emplacement. *Lithos* **58**, 125–43.

Bateman, P. C. 1992. Plutonism in the central part of the Sierra Nevada Batholith, California. *US Geological Survey Professional Paper* **P 1483**.

Bateman, P. C. & Chappell, B. W. 1979. Crystallization, fractionation, and solidification of the Tuolumne Intrusive Series, Yosemite National Park, California. *Geological Society of America Bulletin* **90** (5), 1465–82.

Bateman, P. C. & Nokelberg, W. J. 1978. Solidification of the Mount Givens Granodiorite, Sierra Nevada, California. *Journal of Geology* **86**, 563–79.

Boynton, W. V. 1984. Cosmochemistry of the rare earth elements: meteorite studies. *In* Henderson, P. (ed.) *Rare Earth Element Geochemistry*, 63–114. Amsterdam: Elsevier.

Bracciali, L., Paterson, S. R., Memeti, V., Rocchi, S., Matzel, J. & Mundil, R. 2008. Build-up of the Tuolumne Batholith, California: the Johnson Granite Porphyry. *In LASI 3 Conference Extended Abstract Volume, Physical Geology of Subvolcanic Systems: Laccolith, Sills and Dykes*. Elba Island, Italy, September 2008.

Burgess, S. D. & Miller, J. S. 2008. Construction, solidification, and internal differentiation of a large felsic arc pluton. Cathedral Peak granodiorite, Sierra Nevada Batholith. *In* Zellmer, G. & Annen,

https://doi.org/10.1017/S1755691009016065 Published online by Cambridge University Press

C. (eds) *Geological Society, London, Special Publication* **304**, 203–33. Bath, UK: The Geological Society Publishing House.

Coleman, D. S., Frost, T. P. & Glazner, A. F. 1992. Evidence from the Lamarck Granodiorite for rapid Late Cretaceous crust formation in California. *Science* **258**, 1924–26.

Coleman, D. S., Glazner, A. F., Miller, J. S., Bradford, K. J., Frost, T. P., Joye, J. L. & Bachl, C. A. 1995. Exposure of a Late Cretaceous layered mafic-felsic magma system in the central Sierra Nevada batholith, California. *Contributions to Mineralogy and Petrology* **120**, 129–36.

Coleman, D. S., Walt, G. & Glazner, A. F. 2004. Rethinking the emplacement and evolution of zoned plutons: Geochronologic evidence for incremental assembly of the Tuolumne Batholith, California. *Geology* **32**, 433–6.

Economos, R. C., Miller, J. S., Paterson, S. R., Memeti, V., Erdmann, S. & Žák, J. 2005. The Role of Fractionation at the Emplacement Level in the Tuolumne Batholith, Sierra Nevada, CA. *Geological Society of America Abstracts with Programs* **37**, 554.

Glazner, A. F., Bartley, J. M., Coleman, D. S., Gray, W. & Taylor, R. Z. 2004. Are plutons assembled over millions of years by amalgamation from small magma chambers? *GSA Today* **14**, 4–11.

Glazner, A. F., Coleman, D. S. & Bartley, J. M. 2008. The tenuous connection between high-silica rhyolites and granodiorite plutons. *Geology* **36**, 183–6.

Gray, W. 2003. *Chemical and thermal evolution of the Late Cretaceous Tuolumne Batholith, Yosemite National Park, California*. Ph.D. Thesis. Chapel Hill, University of North Carolina. 202 pp.

Halliday, A. N., Stephens, W. E. & Harmon, R. S. 1980. Rb–Sr and O isotopic relationships in three zoned Caledonian granitic plutons, Southern Uplands, Scotland: evidence for varied sources and hybridisation of magmas. *Journal of the Geological Society, London* **137**, 329–48.

Hill, M., O'Neil, J. R., Noyes, H., Frey, F. A. & Wones, D. R. 1988. Sr, Nd and O isotope variations in compositionally zoned and unzoned plutons in the central Sierra Nevada Batholith. *American Journal of Science* **288–A**, 213–41.

Huber, N. K., Bateman, P. C. & Wahrhaftig, C. 1989. Geologic map of Yosemite National Park and vicinity, California. *US Geological Survey Report* **I-1874**. Scale 1:125,000, 1 sheet.

Hutton, D. H. W. 1992. Granite sheeted complexes: evidence for the dyking ascent mechanism. *Transactions of the Royal Society of Edinburgh: Earth Sciences* **83**, 377–82.

Johnson, S. E., Paterson, S. R. & Tate, M. C. 1999. Structure and emplacement history of multiple-center, cone-sheet-bearing ring complex: the Zarza Intrusive Complex, Baja California, Mexico. *Geological Society of America Bulletin* **111**, 607–19.

Kistler, R. W., Chappell, B. W., Peck, D. L. & Bateman, P. C. 1986. Isotopic variation in the Tuolumne Batholith, central Sierra Nevada: California. *Contributions to Mineralogy and Petrology* **94**, 205–20.

Kistler, R. W. & Fleck, R. J. 1994. Field guide for a transect of the central Sierra Nevada, California: Geochronology and isotope geology. *US Geological Survey Open-File Report* **94-267**, 51 pp.

Lagarde, J. L., Brun, J. P. & Gapais, D. 1990. Formation of epizonal granitic plutons by *in situ* assemblage of laterally expanding magma. *Comptes Rendus de l'Académie des Sciences Paris* **130**, Serie II, 1109–14.

Matzel, J., Mundil, R., Paterson, S. R., Renne, P. & Nomade, S. 2005. Evaluating pluton growth models using high resolution geochronology: Tuolumne Batholith, Sierra Nevada, CA. *Geological Society of America Abstracts with Programs* **37** (7), 131.

Matzel, J., Mundil, R., Miller, J. S., Wooden, J., Mazdab, F., Paterson, S. & Memeti, V. 2007. Zircon growth and recycling during the assembly of the Tuolumne batholith, Sierra Nevada, California. *Goldschmidt Conference Abstracts* **2007**, A639.

McNulty, B. A., Tong, W. & Tobisch, O. T. 1996. Assembly of a dike-fed magma chamber; the Jackass Lakes Pluton, central Sierra Nevada, California. *GSA Bulletin* **108**, 926–40.

Memeti, V., Paterson, S. R., Economos, R. C., Žák, J. & Erdmann, S. 2005. Deciphering Chamber Growth and Internal Magma Chamber Processes Using Magmatic Lobes as Snapshots of Processes During the Construction of the Tuolumne Batholith, Sierra Nevada. *Geological Society of America Abstracts with Programs* **37** (7), 554.

Memeti, V., Paterson, S. R., Matzel, J. & Mundil, R. 2007a. Magmatic lobes as windows into long lived magma chambers: Tuolumne batholith, Sierra Nevada, California. *In* Miller, J. A. & Kisters, A. F. M. (eds) *6th International Hutton Symposium Abstract Volume and Program Guide*. Stellenbosch, South Africa: Department of Geology, Geography and Environmental Sciences, University of Stellenbosch. 236 pp.

Memeti, V., Paterson, S., Matzel, J., Mundil, R., Ducea, M. & Miller, J. 2007b. Dynamics of a magma chamber: Insights into time and length scales of internal processes in the Tuolumne batholith, CA. *Eos Transactions AGU* **88** (52). Fall Meeting Supplement. Abstract V42C-07.

Memeti, V., Paterson, S. R., Matzel, J., Mundil, R. & Okaya, D. In press. Magmatic lobes as "snapshots" of magma chamber growth and evolution in large, composite batholiths: an example from the Tuolumne Intrusion, Sierra Nevada, CA. *Geological Society of America Bulletin*.

Miller, J. S., Glazner, A. F., Farmer, L., Suayah, I. B. & Kieth, L. 2000. A Sr, Nd, and Pb isotopic study of mantle domains and crustal structure from Miocene volcanic rocks in the Mojave Desert, California. *Geological Society of America Bulletin* **112**(8), 1264–79.

Miller, J. S., Matzel, J. E. P., Miller, C. F., Burgess, S. D. & Miller, R. B. 2007. Zircon growth and recycling during the assembly of large, composite arc batholiths. *Journal of Volcanology and Geothermal Research* **167**, 282–99.

Miller, R. B. & Paterson, S. R. 2001. Construction of mid-crustal sheeted plutons: Examples from the north Cascades, Washington. *Geological Society of America Bulletin* **113**, 1423–42.

Paterson, S. R., Okaya, D. & Žák, J. 2003, Thermal histories of episodically constructed, large volume magma chambers: implications for processes along internal contacts: *Geological Society of America Abstracts with Programs* **35**(6), 93.

Paterson, S. R., Vernon, R. H. & Žák, J. 2005. Mechanical Instabilities and Physical Accumulation of K-feldspar Megacrysts in Granitic Magma, Tuolumne Batholith, California, USA. *Journal of the Virtual Explorer* **18**.

Paterson, S. R., Okaya, D., Matzel, J., Memeti, V., Mundil, R. & Nomade, S. 2007. Size and longevity of magma chambers in the Tuolumne Batholith: A comparison of thermal modeling and cooling thermochronology. *Eos Transactions AGU* **88** (52). Fall Meeting Supplement. Abstract V42C-02.

Paterson, S. R., Žák, J. & Janošek, V. 2008. Growth of complex sheeted zones during recycling of older magmatic units into younger: Sawmill Canyon area, Tuolumne batholith, Sierra Nevada, California. *Journal of Volcanology and Geothermal Research* **177** (2), 457–84.

Paterson, S. R. & Miller, R. B. 1998. Mid-crustal magmatic sheets in the Cascades Mountains, Washington: implications for magma ascent. *Journal of Structural Geology* 20, 1345–63.

Paterson, S. R. & Vernon, R. 1995. Bursting the bubble of ballooning plutons; a return to nested diapirs emplaced by multiple processes. *Geological Society of America Bulletin* **107**, 1356–80.

Peck, D. L. 1980. Geologic map of the Merced Peak Quadrangle; central Sierra Nevada, California. *US Geological Survey Report* **GQ-1531**. Scale 1:62,500. 1 sheet.

Pitcher, W. S. & Berger, A. R. 1972. *The Geology of Donegal: a Study of Granite Emplacement and Unroofing*. New York: Wiley. 435 pp.

Ragland, P. C. & Butler, J. R. 1972. Crystallization of the West Farrington Pluton, North Carolina, USA. *Journal of Petrology* **13**, 381–404.

Ratajeski, K., Glazner, A. F. & Miller, B. V. 2001. Geology and geochemistry of mafic to felsic plutonic rocks in the Cretaceous intrusive suite of Yosemite Valley, California. *Geological Society of America Bulletin* **113**(11), 1486–502.

Ratajeski, K., Sisson, T. W. & Glazner, A. F. 2005. Experimental and geochemical evidence for derivation of the El Capitan Granite, California, by partial melting of hydrous gabbroic lower crust. *Contributions to Mineralogy and Petrology* **149**, 713–34.

Reid, J. B., Evans, O. C. & Fates, D. G. 1983. Magma mixing in granitic rocks of the central Sierra Nevada, California. *Earth and Planetary Science Letters* **66**, 243–61.

Sawka, W. N., Chappell, B. W. & Kistler, R. W. 1990. Granitoid compositional zoning by side-wall boundary layer differentiation: evidence from the Palisade Crest Batholith, Central Sierra Nevada, California. *Journal of Petrology* **31**, 519–53.

Scambos, T. A., Loiselle, M. C. & Wones, D. R. 1986. The Center Pond Pluton; the restite of the story (phase separation and melt evolution in granitoid genesis). *American Journal of Science* **286**, 241–80.

Sisson, T. W. 2005. Solidification, Zoning, and Homogenization in Sierran Plutons. *Geological Society of America Abstracts with Programs* **37** (4), 39.

Spera, F. J. & Bohrson, W. A. 2001. Energy-Constrained Open-System Magmatic Processes 1: General Model and Energy-Constrained

Assimilation and Fractional Crystallization (EC-AFC) Formulation. *Journal of Petrology* **42**, 999–1018.

Titus, S. J., Clark, R. & Tikoff, B. 2005. Geologic and geophysical investigation of two fine-grained granites, Sierra Nevada Batholith, California: Evidence for structural controls on emplacement and volcanism. *Geological Society of America Bulletin* **117** (9), 1256–71.

Tobisch, O. T., Saleeby, J. B., Renne, P. R., McNulty, B. A. & Tong, W. 1995. Variations in deformation fields during development of a large-volume magmatic arc, central Sierra Nevada, California. *Geological Society of America Bulletin* **107**, 148–66.

Walawender, M. J., Gastil, R.G., Clinkenbeard, J. P., McCormick, W. V., Eastman, B. G., Wernicke, R. S., Wardlaw, M. S., Gunn, S. H. & Smith, B. M. 1990. Origin and evolution of the zoned La Posta-Type plutons, eastern Peninsular Ranges batholith, southern and Baja California. *In* Anderson, J. L. (ed.) *The Nature and Origin of Cordilleran Magmatism. Geological Society of America Memoir* **174**, 1–18.

Webber, C. E., Candela, P. A., Piccoli, P. M. & Simon, A. C. 2001. Generation of granitic dikes: can texture, mineralogy, and geochemistry be used as guides to determine the mechanism of diking? *Geological Society of America Abstracts with Programs* **33**, A-138.

Weinberg, R. F., Sial, A. N. & Pessoa, R. R. 2001. Magma flow within the Tavares pluton, northeastern Brazil: Compositional and thermal convection. *Geological Society of America Bulletin* **113**, 508–20.

Wiebe, R. A. & Collins, W. J. 1998. Depositional features and stratigraphic sections in granitic plutons: Implications for the emplacement and crystallization of granitic magma. *Journal of Structural Geology* **20**, 1273–89.

Wyborn, D., Chappell, B. W. & James, M. 2001. Examples of convective fractionation in high-temperature granites from the Lachlan Fold Belt. *Australian Journal of Earth Sciences* **48**, 531–41.

Žák, J., Paterson, S. R. & Memeti, V. 2007. Four magmatic fabrics in the Tuolumne batholith, central Sierra Nevada, California (USA): implications for interpreting fabric patterns in plutons and evolution of magma chambers in the upper crust. *GSA Bulletin* **119**, 194–201.

Žák, J. & Paterson, S. R. 2005. Characteristics of internal contacts in the Tuolumne batholith, central Sierra Nevada, California (USA): Implications for episodic emplacement and physical processes in a continental arc magma chamber. *Geological Society of America Bulletin* **117**, 1242–255.

Žák, J. & Paterson, S. R. 2006. Roof and walls of the Red Mountain Creek pluton, eastern Sierra Nevada, California (USA): implications for process zones during pluton emplacement. *Journal of Structural Geology* **28**, 575–87.

MS received 18 February 2008. Accepted for publication 18 September 2008 (Stellenbosch); 15 January 2009 (RSE).